Mechanosensing through Cooperative Interactions between Myosin-II and the Actin Crosslinker Cortexillin-I

Yixin Ren, Janet C. Effler, Melanie Norstrom, Tianzhi Luo, Richard Firtel, Pablo A. Iglesias, Ronald S. Rock, and Douglas N. Robinson

Supplementary Experimental Procedures

Cell Strains

Dictyostelium discoideum strains are presented in Table S1. Constructs were transformed into wild type strain (Ax2 or Ax3:Rep orf+; HS1000) [1], the myosin-II heavy chain null (*myoII*) strain (*mhcA*; HS1) [2], ΔRLC:RLCwt, ΔRLC:RLCS13A [3], *cortexillin-I* null strains (cortIRF and HS1151) [4], and *RacE*^{24EH6} null (and its parental DH1) strain [5] and selected in 1.4x HL5, containing 8% FM (Enriched HL-5) and 15-30 µg/ml G418, 4 µg/ml blasticidin, and/or 15-30 µg/ml hygromycin as appropriate. Actin crosslinkers dynacortin, enlazin, and fimbrin were silenced using RNAi, and knockdown was confirmed by western analysis (not shown) as described previously [6-8].

Tubulin was observed using pDXA-BI: RFP-α-tubulin or pDRH:GFP- or RFP-α-tubulin [9]. Myosin-II was observed by using GFP-myosin-II:pBIG [10], and GFP-3xAla:pBIG and GFP-3xAsp:pBIG constructs [11]. The citrine (enhanced YFP) fluorescent protein labeled myosin-II series was constructed in pDRH for this paper. The citrine cDNA was ligated into the *Bgl* II and *Sal* I sites in pDRH. A *Sac* I site was introduced in the myosin-II heavy chain cDNA at the end of the lever arm as defined in [12]. The myosin-II heavy chain tail was subcloned into the *Sal* I and *Not* I sites of pDRH, with the 5' primer carrying the *Sal* I and *Sac* I sites. The motor mutants were amplified using a 5' primer, which included an in-frame *Sal* I site, and a 3' primer, which included the in-frame *Sac* I site. The two lever arm mutants (2xELCBS and ΔBLCBS) were constructed as defined in [12]. The GRA myosin fragment includes a GFP fused to

the regulatory light chain binding site, which is then linked to the assembly domain [13, 14].

The RFP-cortexillin full-length, RFP-ΔNcortI, RFP-cortI CT, and mCherry-RacE expression plasmids were constructed by first generating RFP- and mCherry-tagging cassettes in pBlueScript, similar to our GFP-tagging system described previously [4, 9]. Once each cDNA was cloned into the respective tagging cassette, the fluorescent protein-fusion cDNAs were subcloned into pDRH for expression in *Dictyostelium*.

Supplementary Analysis

The mechanosensory system involves three apparent elements: load-sensitive motor domain-actin interactions, cortexillin-I-actin anchoring, and myosin-II thick filament assembly dynamics. Here, we deal with the load-sensitivity of the motor domain and the myosin-II thick filament assembly dynamics.

Load sensitivity of the motor domain

From the concentration at the cleavage furrow cortex during cytokinesis, myosin-II reaches concentrations of 5-6 μM and furrow cortex:polar cortex ratios of ~1.6-2. These ratios were originally measured using ratio imaging with volumetric indicators [15]. However, because the myosin-II concentrates along the lateral edges of the cortex, the volumetric normalization offers only a nominal correction [8]. We assessed the concentration ratio of furrow to polar cortex, which agrees directly with the ratio from the volume-corrected analysis (Fig. S5).

With 5-6 μM myosin-II concentration and the volume of the cortex under the micropipette (Fig. S6), this corresponds to 40,000 myosin hexameric monomers (M; each with two motor heads) in the bipolar thick filament (BTF) form in the cortex. We estimate the active surface stress from myosin-II where the myosin-II-generated surface stress (σ) is

$$\sigma = \frac{\text{n heads in BTF form x duty ratio x F/head}}{\text{SA}}$$

where F is the force generated by a myosin head (3 pN), duty ratio is the fraction of myosin heads in the force-generating state as compared to the total number of available heads (assumed to be in the BTF assembled state and is 0.6% for unloaded *Dictyostelium* myosin-II), and SA is the surface area of the cortex under the micropipette. From this, we calculate σ to be 0.04 nN/μm^2, which agrees with the active radial stresses at the cleavage furrow (0.04-0.1 nN/μm^2) determined previously [16]. However, for

accumulation of myosin-II to the micropipette, 0.4-0.6 nN/μm^2 pressure was required. If the myosin-II heads are recruited into the load-bearing state to directly off-set the applied pressure, then the myosin-II could reasonably undergo a 5-10-fold shift in duty ratio (0.4 nN/μm^2/0.04 nN/μm^2), which compares well with the load-dependent shifts in duty ratio observed for other myosin-II enzymes [17, 18].

Myosin-II thick filament assembly

Our data indicate that myosin-II must be able to undergo full assembly-disassembly in order to accumulate during the mechanosensory response. These observations suggest that there is likely to be a mechanosensitive step during thick filament assembly. The assembly pathway and the kinetic parameters are largely known.

$$
\begin{array}{rcll}
M_0 & \underset{k_{-1}}{\overset{k_1}{\rightleftharpoons}} & M, & k_1 = 0.0008\,\mathrm{s}^{-1} \\
 & & & k_{-1} = 0.1\,\mathrm{s}^{-1} \\
M + M & \underset{k_{-2}}{\overset{k_2}{\rightleftharpoons}} & D, & k_2 = 0.37\,\mu\mathrm{M}^{-1}\mathrm{s}^{-1} \\
 & & & k_{-2} = 0.01\,\mathrm{s}^{-1} \\
D + D & \underset{k_{-3}}{\overset{k_3}{\rightleftharpoons}} & T, & k_3 = 0.0395\,\mu\mathrm{M}^{-1}\mathrm{s}^{-1} \\
 & & & k_{-3} = 0.0045\,\mathrm{s}^{-1} \\
T + D & \underset{k_{-4}}{\overset{k_4}{\rightleftharpoons}} & BTF_3, & k_4 = 1.25\,\mu\mathrm{M}^{-1}\mathrm{s}^{-1} \\
 & & & k_{-4} = 0.025\,\mathrm{s}^{-1} \\
BTF_n + D & \underset{k_{-5}}{\overset{k_5}{\rightleftharpoons}} & BTF_{n+1}, & k_5 = 10\,\mu\mathrm{M}^{-1}\mathrm{s}^{-1} \\
 & & & k_{-5} = 0.2\,\mathrm{s}^{-1}
\end{array}
$$

M_0 is the assembly incompetent (stabilized in part by heavy chain phosphorylation) hexameric monomer, M is the assembly-competent monomer, D is the parallel dimer, T is anti-parallel tetramer, which is thought to be the first stable nucleus, and BTF_n is the bipolar thick filament with n dimers. We consider BTFs that include 3 to

36 dimers. The rates for conversion between M_0 and M were chosen so that, at steady state, M_0 accounts for approximately 80% of total myosin [19]. Rates for k_2, k_{-2}, k_3, k_{-3}, k_4 and k_{-4} are derived from [20, 21]. The value of k_{-5} is derived from fluorescence recovery after photobleaching analysis [8, 22]. We also make the assumption that every time a dimer is added or released, the probability of further addition/removal is the same. Simulations based on this model were used to determine where the system is most sensitive. First, we allowed the myosin BTFs to assemble until steady state was reached. Then, to determine where force generation can have an appreciable effect on BTF concentration, we perturbed all 10 kinetic parameters in the model 10-fold, which was the amount estimated from the potential shift in duty ratio and strongly bound state time estimated above. The greatest effect was found to be in the rates between M and M_0. A ten-fold decrease in k_{-1} resulted in a ~50% increase in myosin found in the BTF after 60 s (Fig. S7). To mimic the 3xAla mutants, we also eliminated the assembly incompetent hexamer, M_0. In this case, the effect of changing other parameters was negligible, because at this point, nearly all the myosin is already in BTF form. Finally, we present the time-course for simulated assembly, which occurred on the minute time-scale, and the distribution of sizes of BTFs at 60 s compared to the initial steady state.

Three conclusions may be drawn from this analysis. First, the largest impact on the assembly dynamics comes from changing the rates of converting M_0 to M. This could occur because myosin motor binding to actin polymers is highly cooperative. By stabilizing motor domains on the actin this may allow free M to bind the actin placing them in close proximity for assembly into BTFs. It is notable that at steady state, our simulations indicate that most of the thick filaments do not reach the full 72 mer size [20]. Rather they populate a distribution of intermediate sizes of BTFs, which is similar to previous simulations of the assembly of muscle myosin thick filaments [23]. Therefore, it is likely that when new M binds the actin polymers they directly insert into pre-existing

BTFs. Moreover, the addition of actin polymers to myosin-II BTF assembly reactions *in vitro* eliminates the lag-phase characteristic of the nucleation phase [20]. This observation has interesting implications for myosin-II recruitment in other scenarios as well. For example, myosin-II may typically exist as a mixture of intermediate BTF sizes so that when signals trigger accumulation, the free monomers just have to incorporate directly into the BTFs. Myosin heavy chain phosphorylation then would ensure that the system relaxes back to the initial steady state distribution after the accumulation signal terminates. Second, these simulations demonstrate that 3xAla myosin-II would not respond to mechanical stress because there is insufficient available free M to respond. Third, these simulations offer one explanation why myosin-II accumulation in response to mechanical load requires one to a couple of minutes; the kinetic parameters for myosin BTF assembly are set to require that amount of time for accumulation. However, it is important to bear in mind that this analysis is not intended to be a full treatment of the system as it clearly does not include other aspects such as cytoplasmic viscosity, cortexillin-I dynamics, and membrane/cortex surface and curvature.

Supplementary References

1. Robinson, D.N., Ocon, S.S., Rock, R.S., and Spudich, J.A. (2002). Dynacortin is a novel actin bundling protein that localizes to dynamic actin structures. J. Biol. Chem. *277*, 9088-9095.
2. Ruppel, K.M., Uyeda, T.Q.P., and Spudich, J.A. (1994). Role of highly conserved lysine 130 of myosin motor domain. In vivo and in vitro characterization of site specifically mutated myosin. J. Biol. Chem. *269*, 18773-18780.
3. Chen, P., Ostrow, B.D., Tafuri, S.R., and Chisholm, R.L. (1994). Targeted disruption of the *Dictyostelium* RMLC gene produces cells defective in cytokinesis and development. J. Cell Biol. *127*, 1933-1944.
4. Robinson, D.N., and Spudich, J.A. (2000). Dynacortin, a genetic link between equatorial contractility and global shape control discovered by library complementation of a Dictyostelium discoideum cytokinesis mutant. J. Cell Biol. *150*, 823-838.
5. Larochelle, D.A., Vithalani, K.K., and DeLozanne, A. (1996). A novel member of the *rho* family of small GTP-binding proteins is specifically required for cytokinesis. J. Cell Biol. *133*, 1321-1329.

6. Girard, K.D., Chaney, C., Delannoy, M., Kuo, S.C., and Robinson, D.N. (2004). Dynacortin contributes to cortical viscoelasticity and helps define the shape changes of cytokinesis. EMBO J. *23*, 1536-1546.
7. Octtaviani, E., Effler, J.C., and Robinson, D.N. (2006). Enlazin, a natural fusion of two classes of canonical cytoskeletal proteins, contributes to cytokinesis dynamics. Mol. Biol. Cell *17*, 5275-5286.
8. Reichl, E.M., Ren, Y., Morphew, M.K., Delannoy, M., Effler, J.C., Girard, K.D., Divi, S., Iglesias, P.A., Kuo, S.C., and Robinson, D.N. (2008). Interactions between myosin and actin crosslinkers control cytokinesis contractility dynamics and mechanics. Curr. Biol. *18*, 471-480.
9. Effler, J.C., Kee, Y.-S., Berk, J.M., Tran, M.N., Iglesias, P.A., and Robinson, D.N. (2006). Mitosis-specific mechanosensing and contractile protein redistribution control cell shape. Curr. Biol. *16*, 1962-1967.
10. Moores, S.L., Sabry, J.H., and Spudich, J.A. (1996). Myosin dynamics in live Dictyostelium cells. Proc. Natl. Acad. Sci. USA *93*, 443-446.
11. Sabry, J.H., Moores, S.L., Ryan, S., Zang, J.-H., and Spudich, J.A. (1997). Myosin heavy chain phosphorylation sites regulate myosin localization during cytokinesis in live cells. Mol. Biol. Cell *8*, 2647-2657.
12. Uyeda, T.Q., Abramson, P.D., and Spudich, J.A. (1996). The neck region of the myosin motor domain acts as a lever arm to generate movement. Proc. Natl. Acad. Sci. USA *93*, 4459-4464.
13. Zang, J.-H., and Spudich, J.A. (1998). Myosin II localization during cytokinesis occurs by a mechanism that does not require its motor domain. Proc. Natl. Acad. Sci. USA *95*, 13652-13657.
14. Hostetter, D., Rice, S., Dean, S., Altman, D., McMahon, P.M., Sutton, S., Tripathy, A., and Spudich, J.A. (2004). Dictyostelium myosin bipolar thick filament formation: importance of charge and specific domains of the myosin rod. PLoS Biol. *2*, e356.
15. Robinson, D.N., Cavet, G., Warrick, H.M., and Spudich, J.A. (2002). Quantitation of the distribution and flux of myosin-II during cytokinesis. BMC Cell Biology *3*, 4.
16. Zhang, W., and Robinson, D.N. (2005). Balance of actively generated contractile and resistive forces controls cytokinesis dynamics. Proc. Natl. Acad. Sci. USA *102*, 7186-7191.
17. Kovacs, M., Thirumurugan, K., Knight, P.J., and Sellers, J.R. (2007). Load-dependent mechanism of nonmuscle myosin 2. Proc. Natl. Acad. Sci. USA *104*, 9994-9999.
18. Veigel, C., Molloy, J.E., Schmitz, S., and Kendrick-Jones, J. (2003). Load-dependent kinetics of force production by smooth muscle myosin measured with optical tweezers. Nat. Cell Biol. *5*, 980-986.
19. Egelhoff, T.T., Lee, R.J., and Spudich, J.A. (1993). *Dictyostelium* myosin heavy chain phosphorylation sites regulate myosin filament assembly and localization *in vivo*. Cell *75*, 363-371.
20. Mahajan, R.K., and Pardee, J.D. (1996). Assembly mechanism of *Dictyostelium* myosin II: Regulation by K^+, Mg^{2+}, and actin filaments. Biochemistry *35*, 15504-15514.
21. Moores, S.L., and Spudich, J.A. (1998). Conditional Loss-of-Myosin-II-Function Mutants Reveal a Position in the Tail that Is Critical for Filament Nucleation. Mol. Cell *1*, 1043-1050.
22. Yumura, S., Yoshida, M., Betapudi, V., Licate, L.S., Iwadate, Y., Nagasaki, A., Uyeda, T.Q., and Egelhoff, T.T. (2005). Multiple myosin II heavy chain kinases:

roles in filament assembly control and proper cytokinesis in Dictyostelium. Mol. Biol. Cell *16*, 4256-4266.
23. Davis, J.S. (1993). Myosin thick filaments and subunit exchange: A stochastic simulation based on the kinetics of assembly. Biochemistry *32*, 4035-4042.

Supplementary Figures

Fig. S1. Wild type myosin-II assembly dynamics are required for the mechanosensory response. Time series (times in s) of DIC and fluorescence images are shown for (A) a *myoII*: GFP-3xAsp cell; (B) a *myoII*: GFP-3xAla cell; (C) three different *myoII:* GFP-RLCBS-AD (GRA) cells expressing varying amounts of GFP-GRA and aspirated using pressures of 0.39, 0.44 and 0.51 nN/μm^2, respectively, and (D) a RLC: RLC(S13A);GFP-myoII. Frequency histograms show measurements from all cells measured for each genotype. As described in the Methods, the dark grey bars of the histograms indicate positive responses, while light grey bars indicate negative responses. Scale bar, 10 μm.

Fig. S2. Summary of myosin-II mutants analyzed and a comparison of their requirements for mechanosensing vs. cytokinesis. Pressure, P.

Fig. S3. Frequency histograms showing the responses of wild type, ΔBLCBS, 2xELC and S456L myosin-II motors at the indicated pressures. These data in panel (A) are summarized in Fig. 1D in the main text. While the intensities are easily separated as responses and non-responses as described in the Methods, for an independent check we present the pressure dependency of the mean log[Ip/Io] (±SEM) values for the entire datasets (B). This approach considers all of the measurements without added assumptions and in this presentation, the data still fall into three classes according to lever arm length (2xELC, wild type and ΔBLCBS). Student's *t*-test results are included in Fig. 1 legend in the main text.

Fig. S4. Actin crosslinkers dynacortin, fimbrin, and enlazin are not required for mechanosensing. Cells expressing GFP-myosin-II and RFP-tubulin had dynacortin,

enlazin or fimbrin silenced by RNA interference (see Supplementary Methods). Arrows show the responses. Scale bar, 10 μm.

Fig. S5. GFP-myosin-II distribution vs. time. Time is in minutes. D_x represents a distance of 2.7 μm, which was set to time 0 as described [16]. Ratio of average GFP-myosin-II intensity in the furrow cortex relative to the average intensity of the polar cortex was measured every 15 seconds (blue line). Two-color images reveal the mitotic spindle (RFP-tubulin) and GFP-myosin-II localization at each time-point. Data are based on n=10 cells; the curve is the average±SEM. The intensity ratios of 1.4-2 observed in the micropipette (Fig. S6) are comparable to the intensity ratios observed at the cleavage furrow cortex.

Fig. S6. Dimensions of the hemispherical cap, radial myosin-II intensity and kinetics of myosin-II accumulation at the micropipette. (A) The geometry of the cortex in the micropipette. Here we assume the cortex is 0.35-μm thick comparable to other measurements. From this, the volume of the cytoplasm in the hemispherical cap is 22 μm^3, and the volume of the hemispherical cap cortex is 11 μm^3. The surface area of the hemisphere is 40 μm^2. (B) The circumferential line plot shows the Cit-wild type myosin-II signal intensity around the cortex measured for 9 responding cells. The 0 μm corresponds to the 0 point in panel A. The global average intensity ratio in the hemispherical cortex (from -4 to 4 μm) is 1.5±0.42 (mean±SD, n=410). (C) To detail the kinetics of the response, we analyzed the time required for the peak response to occur. Graph shows an example time-course. From the start of the movie, there is a lag time before any myosin-II accumulation is detectable, and the response time is the time required for the signal to rise from baseline to the peak. The total time is the time from

the start of the experiment to the peak. For this kinetic analysis, we normalized the intensity in the pipette (Ip) to the local intensity of the cytoplasm (Ic). This region was more dependably in focus at each time point. As a result, the response ratio is a little lower than when normalizing to the opposite cortex (Io). The mean±SEM times and the range of the times are provided for each phase. The dataset is based on the same 9 cells as analyzed for panel B.

Fig. S7. Simulation and sensitivity analysis reveals a potential force-sensitive step in myosin-II bipolar thick filament assembly. (A) Graph shows that a 10-fold change in k_1 yields a 50% increase in assembled myosin-II. 3xAla is already nearly completely assembled, preventing further force-sensitive assembly. (B) Graph shows that force-induced assembly occurs on the minute time-scale. Time 0 shows the initial steady state before k_{-1} is shifted down 10-fold (to mimic the impact of force). By 60 s, the concentration of myosin in BTF form is increased 1.5-fold, similar to that observed in the micropipette. (C) Graph shows the distribution of BTF sizes before (without force – steady state) and 60 s after (with force – pre-steady state) the 10-fold change in k_{-1}. Shifting k_{-1} increases the average size of the BTFs.

Table S1. *Dictyostelium* strains used in this study

Strain	Genotype	Question	# Responses/ Total Cells
myoII:: RFP-α-tubulin; GFP-myoII; pLD1	*myoII*(HS1)::RFP-α-tubulin,Bl^R:pDXA-Bl; GFP-myoII, Hyg^R: pDRH; pLD1,$G418^R$: pLD1A15SN	Influence of crosslinkers on mechanosensory response	1/4
myoII:: RFP-α-tubulin; GFP-myoII; dynhp	*myoII*(HS1)::RFP-α-tubulin,Bl^R:pDXA-Bl; GFP-myoII, Hyg^R: pDRH; dynhp,$G418^R$: pLD1A15SN		2/4
myoII:: RFP-α-tubulin; GFP-myoII;fimhp	*myoII*(HS1)::RFP-α-tubulin,Bl^R:pDXA-Bl; GFP-myoII, Hyg^R: pDRH; fimhp,$G418^R$: pLD1A15SN		6/13
myoII:: RFP-α-tubulin; GFP-myoII; enlhp	*myoII*(HS1)::RFP-α-tubulin,Bl^R:pDXA-Bl; GFP-myoII, Hyg^R: pDRH; enlhp,$G418^R$: pLD1A15SN		4/7
myoII::GFP-cortI	*myoII*(HS1)::GFP-cortI,Hyg^R:pDRH; $G418^R$:pLD1A15SN	Cortexillin-I dependency on myosin-II	0/15
myoII:: GFP-cortI; dynhp	*myoII*(HS1)::GFP-cortI,Hyg^R:pDRH; dynhp,$G418^R$:pLD1A15SN		0/13
myoII:: GFP-cortI; S456L	*myoII*(HS1)::GFP-cortI,Hyg^R:pDRH; S456L,$G418^R$:pBIG		1/13
myoII:: GFP-cortI; myoII	*myoII*(HS1)::GFP-cortI,Hyg^R:pDRH; myoII, $G418^R$:pBIG		14/32
KAx3:: GFP-myoII; RFP-α-tubulin	KAx3::RFP-α-tubulin, Hyg^R:pDRH; GFP-myoII, $G418^R$: pBIG	Wild type parent of *cortI*(RF) strain	6/7
cortI:: GFP-myoII; RFP-α-tubulin	*cortI*(RF)::RFP-α-tubulin, Hyg^R:pDRH; GFP-myoII, $G418^R$: pBIG	Myosin-II dependency on cortexillin-I	0/10
cortI:: GFP-myoII; RFP-ΔNcortI	*cortI(RF)::* RFP-ΔNcortI, Hyg^R:pDRH; GFP-myoII, $G418^R$: pBIG		6/19
cortI:: GFP-myoII; RFP-cortI	*cortI(RF)::* RFP-cortI, Hyg^R:pDRH; GFP-myoII, $G418^R$: pBIG		7/10
$cortI^{1151}$:: GFP-myoII; RFP-α-tubulin	$cortI^{1151}$::RFP-α-tubulin,Hyg^R:pDRH;GFP-myoII, $G418^R$: pBIG		0/15
$cortI^{1151}$:: GFP-myoII; RFP-cortICT	$cortI^{1151}$:: RFP-cortICT,Hyg^R:pDRH; GFP-myoII,$G418^R$: pBIG		1/13
$cortI^{1151}$:: GFP-myoII; RFP-cortI	$cortI^{1151}$:: RFP- cortI,Hyg^R:pDRH; GFP-myoII,$G418^R$: pBIG		5/8

Strain	Genotype	Question	# Responses/ Total Cells
myoII: RFP-α-tubulin; GFP-myoII	*myoII*(HS1)::GFP-myoII, G418^{R}:pBIG; RFP-α-tubulin, Hyg^{R}: pDRH	Assembly dynamics (wild type control)	16/26*
myoII: RFP-α-tubulin; GFP-GRA	*myoII*(HS1)::GFP-RLCBS-Assembly Domain; RFP-α-tubulin, Hyg^{R}: pDRH	Sufficiency of minimal cleavage furrow targeting domain	0/6
myoII: RFP-α-tubulin; GFP-3xAsp	*myoII*(HS1)::GFP-3xAsp myoII, G418^{R}:pBIG; RFP-α-tubulin, Hyg^{R}:pDRH	Myosin assembly dynamics	0/10
myoII: RFP-α-tubulin; GFP-3xAla	*myoII*(HS1)::GFP-3xAla myoII, G418^{R}:pBIG; RFP-α-tubulin, Hyg^{R}:pDRH	Myosin disassembly dynamics	0/16
RLC: RLC-S13A; GFP-myoII	*ΔRLC:* RLC-S13A, G418^{R}; GFP-myoII, Hyg^{R}: pDRH	Role of myosin RLC phosphorylation	2/19
RLC: RLC; GFP-myoII	*ΔRLC:* RLC (wt), G418^{R}; GFP-myoII, Hyg^{R}: pDRH		7/11
myoII: GFP-α-tubulin; Citrine-myoII	*myoII*(HS1)::Cit-myoII, Hyg^{R}:pDRH; GFP-α-tubulin, G418^{R}:pDEX	Role of myosin-II mechanochemistry and wild type 9-nm lever arm (wild type control)	ΔP15 mm – 3/20 ΔP40 mm – 10/21 ΔP65 mm – 9/15
myoII: GFP-α-tubulin; Citrine-S456L myoII	*myoII*(HS1)::Cit-myoII (S456L), Hyg^{R}:pDRH; GFP-α-tubulin, G418^{R}:pDEX	Role of myosin-II mechanochemistry	ΔP15 mm – 1/10 ΔP40 mm – 11/37 ΔP65 mm – 9/17
myoII: GFP-α-tubulin; Citrine-ΔBLCBS myoII	*myoII*(HS1)::Cit-myoII (ΔBLCBS), Hyg^{R}:pDRH; GFP-α-tubulin, G418^{R}:pDEX	2-nm long lever arm	ΔP15 mm – 1/10 ΔP40 mm – 8/34 ΔP65 mm – 13/33
myoII: GFP-α-tubulin; Citrine-2xELC myoII	*myoII*(HS1)::Cit-myoII (2xELC), Hyg^{R}:pDRH; GFP-α-tubulin, G418^{R}:pDEX	13-nm long lever arm	ΔP15 mm – 8/18 ΔP40 mm – 9/17 ΔP65 mm – 10/15
RacE: GFP-myoII; RFP-α-tubulin	*RacE^{24EH6}::*GFP-myoII G418^{R}:pBIG; RFP-α-tubulin, Hyg^{R}:pDRH	RacE inhibition of mechanosensory response	Mitotic – 2/5 Interphase – 23/37
RacE: GFP-myoII; mCherry-RacE	*RacE^{24EH6}::*GFP-myoII G418^{R}:pBIG; mCherry-RacE, Hyg^{R}, pDRH		Interphase – 2/20
RacE: GFP-cortI	*RacE^{24EH6}::*GFP-cortI; G418^{R}: pEXP4		Interphase – 15/37

*Ref [9].

Supplemental Figure S1

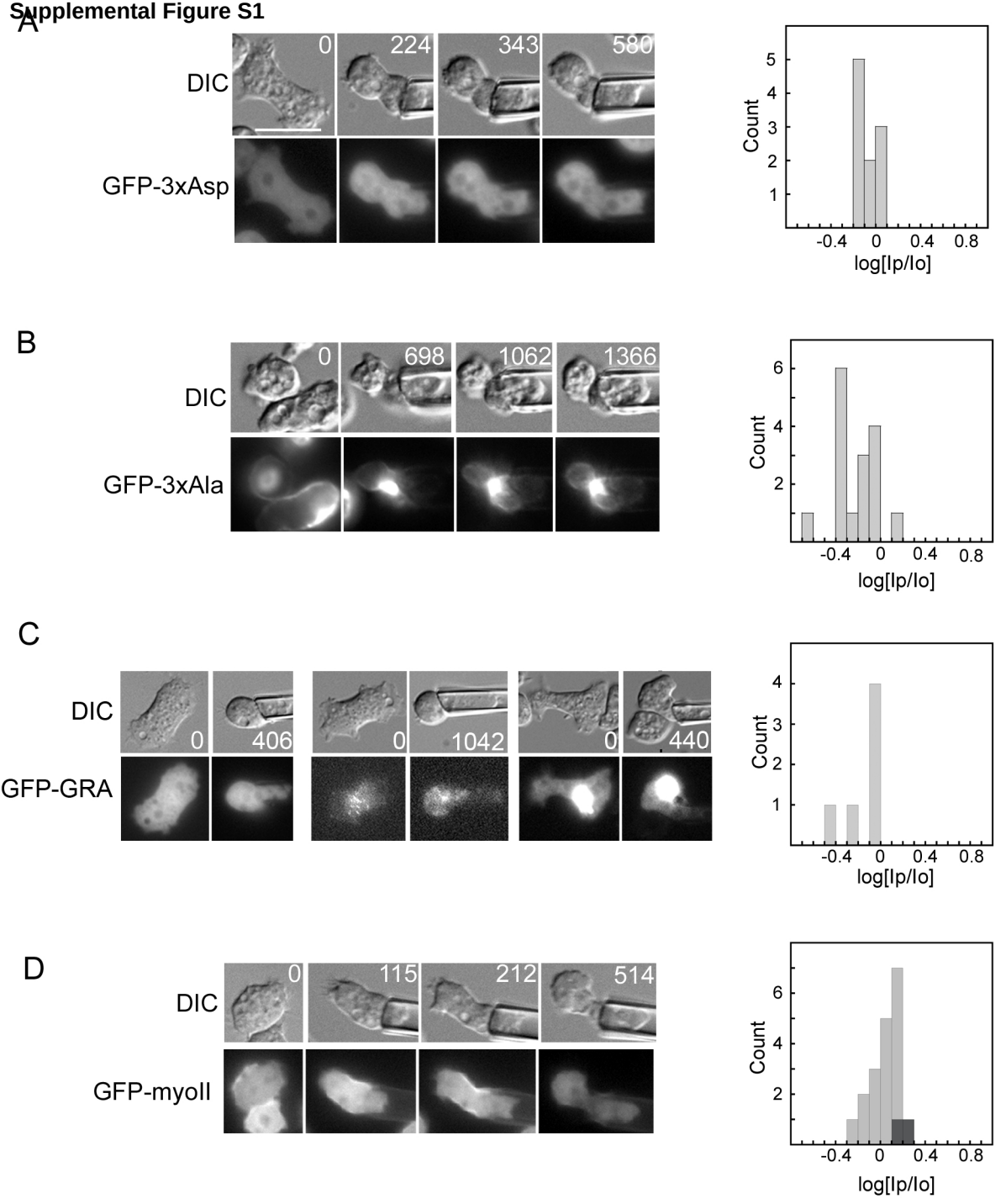

Fig. S1

Supplemental Figure S2

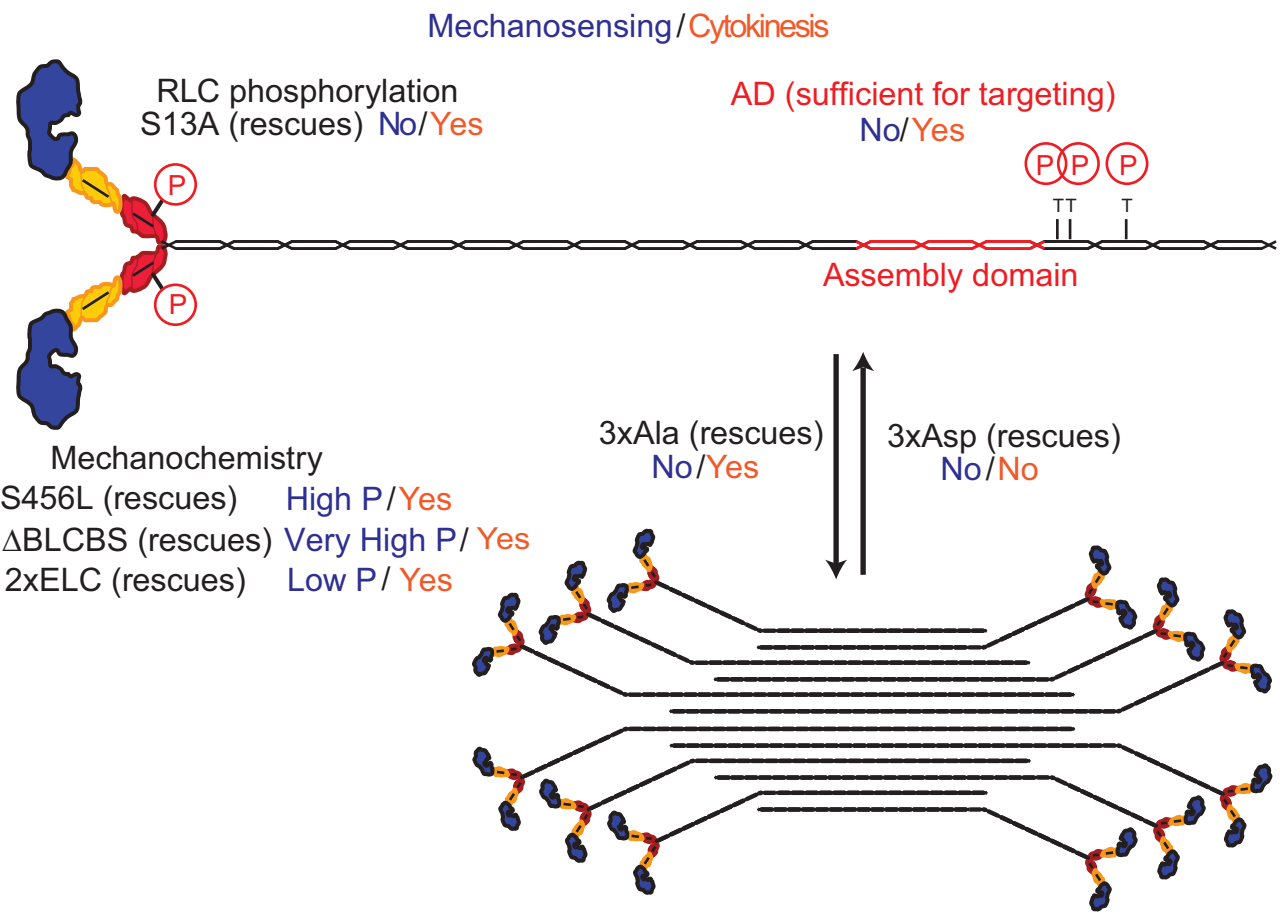

Fig. S2

Supplemental Figure S3

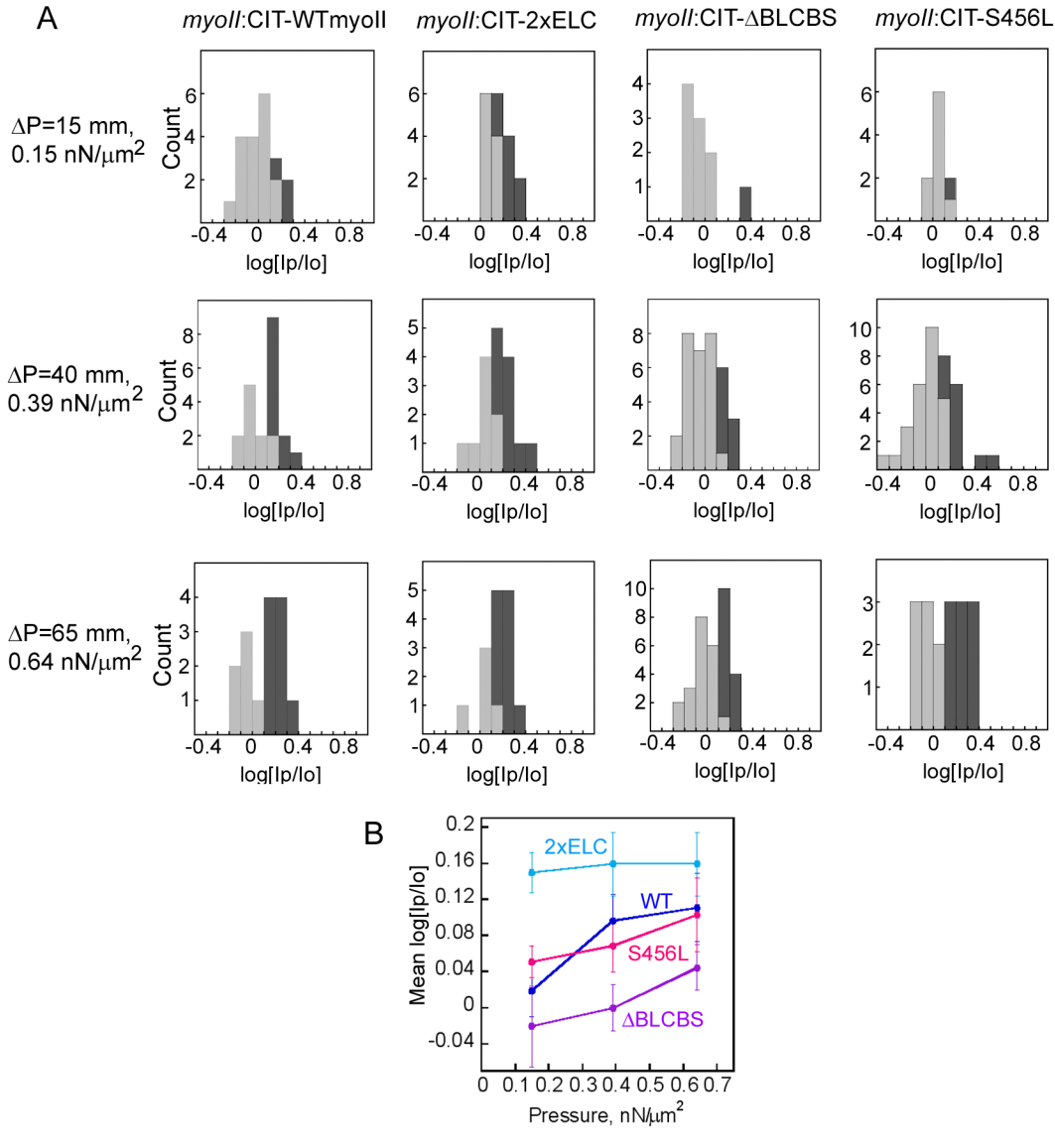

Fig. S3

Supplemental Figure S4

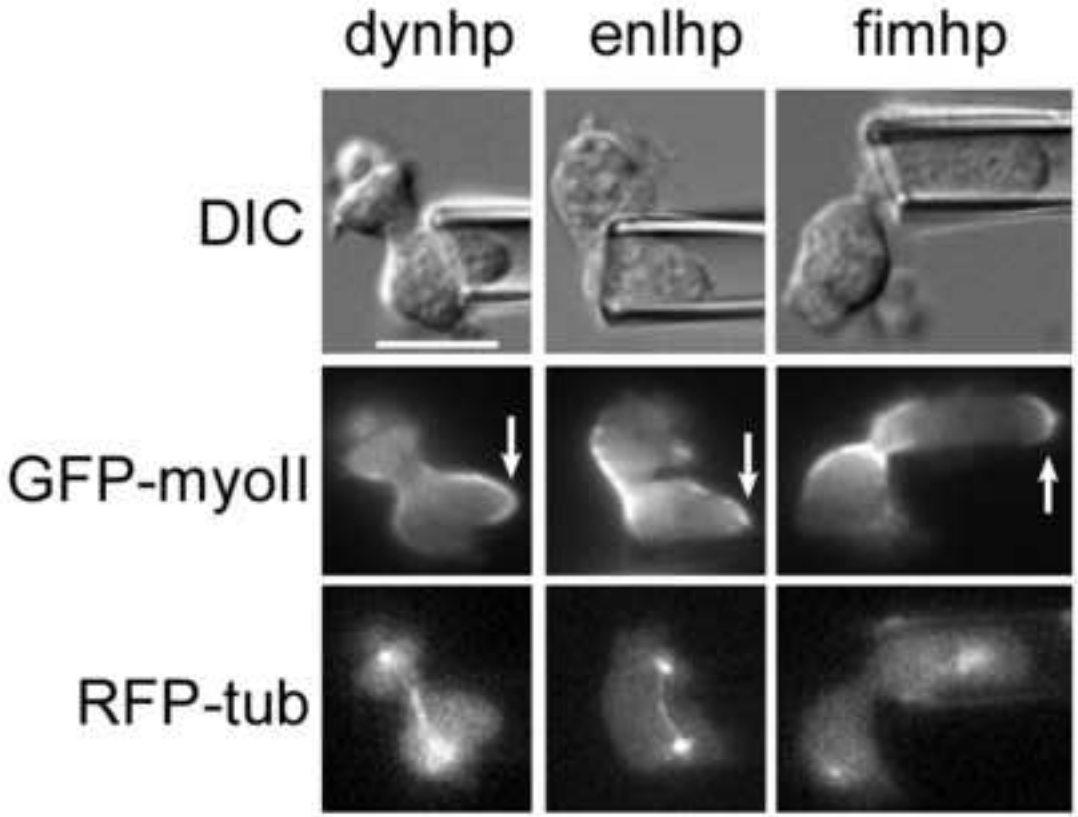

Fig. S4

Supplemental Figure S5

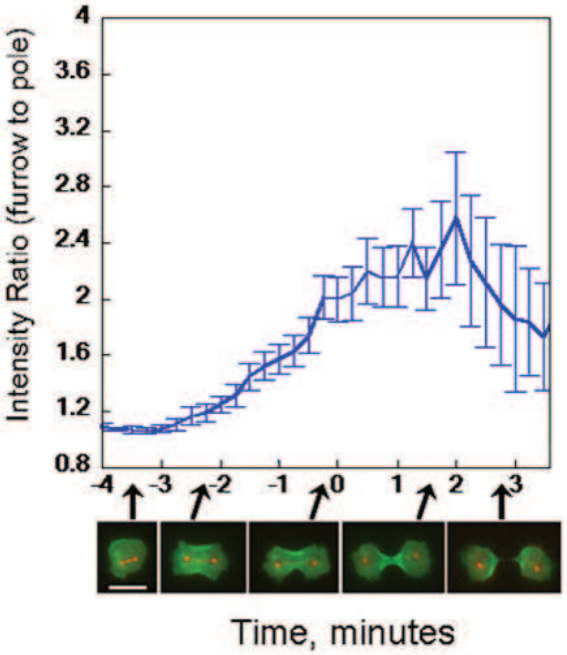

Fig. S5

Supplemental Figure S6

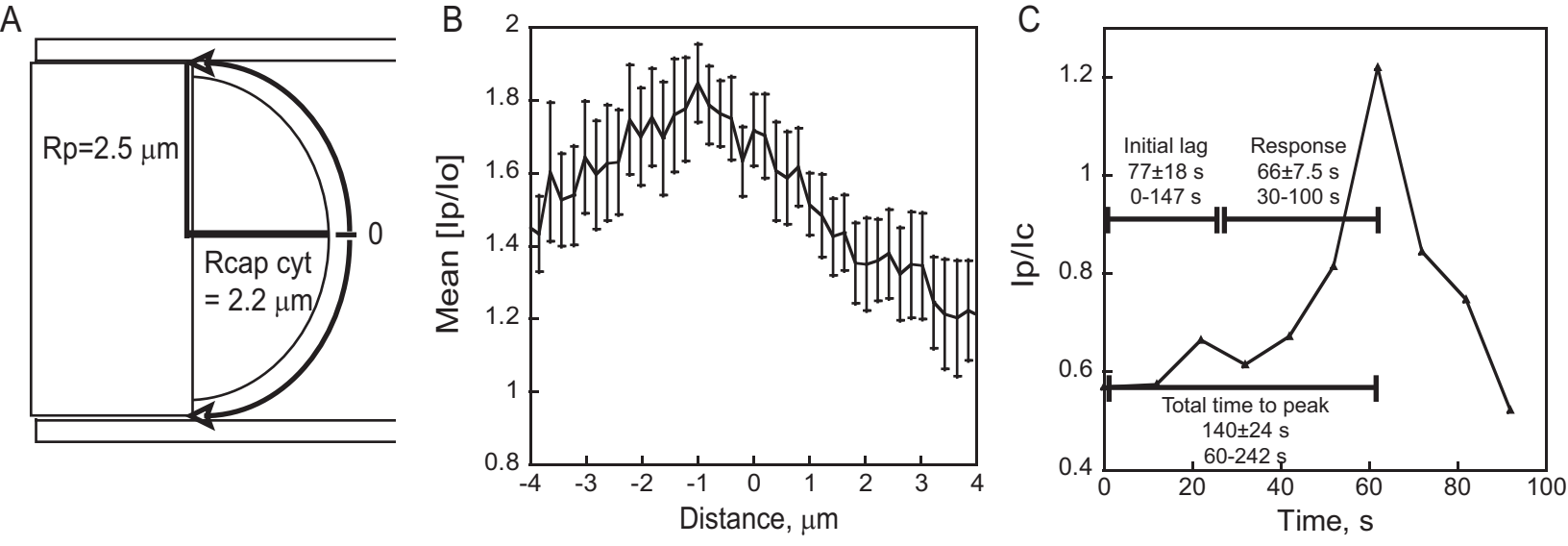

Fig. S6

Supplemental Figure S7

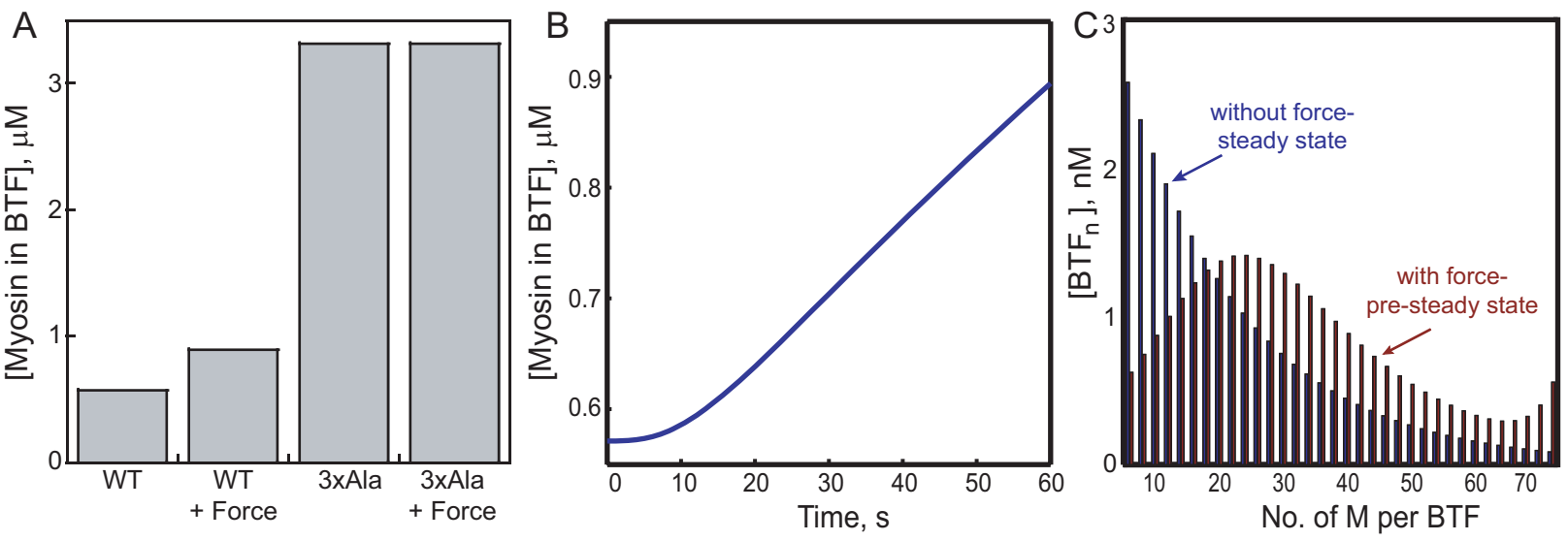

Fig. S7